

Ballistic Showers During Crater Peak Eruptions of Mount Spurr Volcano, Summer 1992

By Richard B. Waitt, Larry G. Mastin, and Thomas P. Miller

CONTENTS

Abstract	89
Introduction	89
Character of projectiles	90
Properties	90
Uneven temperatures	94
Impact craters	94
Relation to wind, distinction from proximal fall	95
Reconstructed velocities of ballistic projectiles	96
Method	96
Drag	97
Discussion	102
Factors besides drag	103
Discussion	104
Hydrovolcanic nature of explosions	104
Horizontally curving trajectories	104
References cited	105

ABSTRACT

Crater Peak vent at Mount Spurr volcano in Alaska ejected large ballistic blocks and bombs southeast from the vent near the end of the August 18, 1992, subplinian eruption. This eruption produced the most extensive bombfield of the 1992 eruptions. Lithic and juvenile andesite ballistic projectiles range in diameter from less than 10 cm to 2 m, and they range in density from 1.20 to 2.75 g/cm³. Lithic ballistic clasts are angular and blocky while cauliflower bombs are common among juvenile clasts, both typical of hydromagmatic explosions. As the eruption waned, ground water from the cone may have poured into the vent along with *ejecta* fallback and talus to fuel hydromagmatic explosions.

We estimate initial velocity needed to eject blocks to the observed 2 to 4 km and more from the vent by iteratively calculating the points of hypothetical trajectories. Drag influences the range of the blocks but is poorly constrained for irregularly shaped volcanic ballistics because it varies enormously with various combinations of shape, orientation, roughness, and velocity. For ballistics of 25 cm and larger that landed within 3.5 km of the vent, drag coefficients vary between 0.06 and 1.5 for spheres and cubes, and they

yield calculated vent velocities of 155 to 840 m/s; smaller and more distal clasts yield values improbably as much as several times higher. Ballistics larger than 10 cm apparently traveled much of their trajectories in a range of very high Reynolds numbers, between 4×10^5 and 1×10^7 , where drag on smooth spheres is as low as 0.06. In contrast to previous studies on volcanic ballistics, we infer that with low drag coefficients relatively small ballistic clasts can achieve fairly long range even with moderate ejection velocities.

Many impact craters along the southeast azimuth from the vent are aligned not directly southeastward but more nearly south. This southward deviation is typically 20° to 40°, the maximum deviation 67°—despite westerly wind that tended to shift trajectories east. A pitched baseball curves in the direction of applied spin (*Magnus effect*). Thus many projectiles apparently had strong angular velocity about near-vertical axes. The deviant projectiles at Crater Peak apparently acquired clockwise spin (when viewed from above) while being ejected from the vent.

INTRODUCTION

Crater Peak vent at Mount Spurr volcano ejected large ballistic blocks and bombs during all three eruptions of 1992. Ballistics flew north during the June 27 eruption, east-southeast during the August 18 eruption, and east during the September 16–17 eruption. The bombfield of the August eruption, which is scattered over an area of at least 12 square kilometers and extends more than 8 km east-southeast of the vent (figs. 1, 2, 3), is the most extensive and accessible bombfield of the 1992 eruptions.

Between the June 27 and August 18 eruptions, the vent shifted to the northwesternmost part of the crater, tight against and even slightly beneath the steep northwest (southeast-facing) crater wall (fig. 2). This position promoted ejection of debris preferentially southeastward. Thus pyroclastic flows of the August eruption were launched over the southeast crater rim rather than flowing south through a deep, wide breach in the crater rim (fig. 2) (Miller and others, this volume; Waitt, this volume).

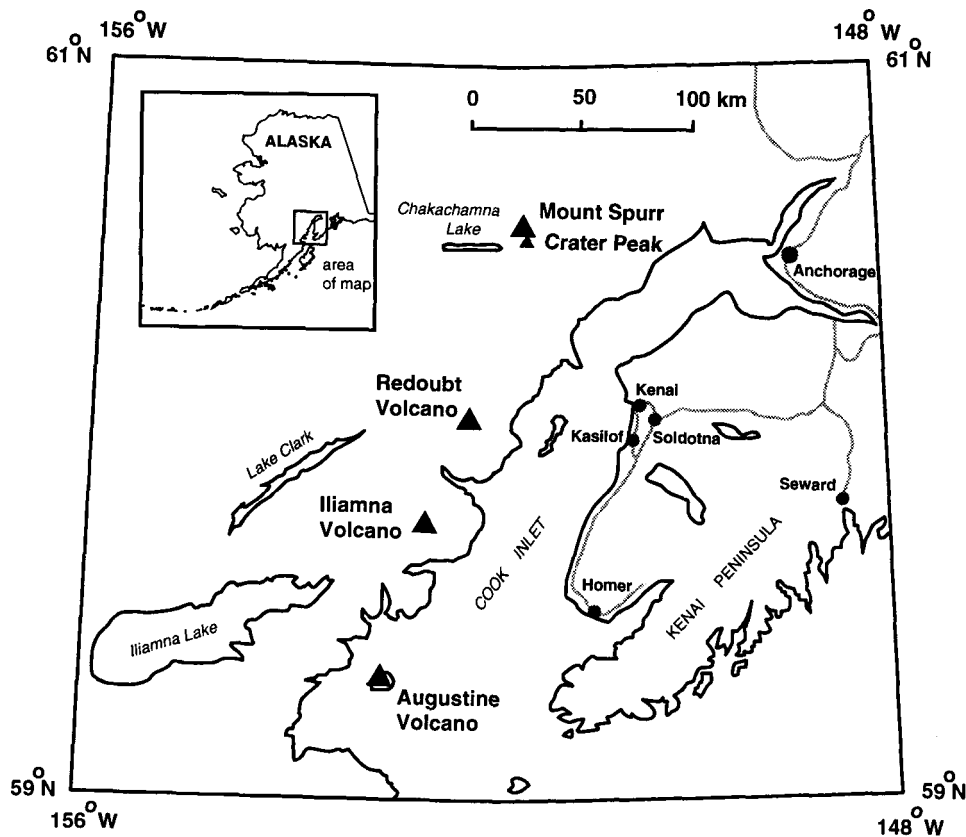


Figure 1. Index map of Cook Inlet area, Alaska, showing location of Mount Spurr volcano.

On the southeast flank of Crater Peak cone the August 18 bombfield comprises thousands of craters, bombs, and bomb fragments. Visible on 1:30,000-scale aerial photographs, the largest (>2 m diameter) and most concentrated craters extend up to altitude 1,375 m (4,500 ft) at range 1.8 km southeast of the vent. Above that level the slope consists of rock and is too steep for bombs to make impact craters. The abundantly cratered part of the field extends down to altitude 835 m (2,740 ft) at range 3.4 km from the vent. The density of large (2–5 m diameter) bomb craters is five per 100 square meters, estimated from aerial photographs. The actual number of bombs and craters including those below the resolution of the photographs (less than 2 m diameter) is at least an order of magnitude larger.

From field and aerial-photograph observations at several adjacent sites at range about 3.3 km, nearly as many large impact craters (>1 m diameter) per unit area are apparent on pyroclastic-flow deposits of the August eruption as just beyond flow margins. At range 8 km where the ballistics overlapped the field of continuous subplinian fall, the ballistics formed small craterlets in the much finer grained fall deposit. Therefore most of the ballistics came near the end of the

eruption after pyroclastic-flow and fall deposits were emplaced. Yet near range 3.3 km a pyroclastic-flow margin overlapped two impact craters, and so some of the ballistics clearly fell before the most extensive pyroclastic flows had occurred.

CHARACTER OF PROJECTILES

PROPERTIES

Ballistic projectiles range in diameter from about 2 m to 8 cm or less. Those larger than 30 cm are lithic. About half the projectiles smaller than 15 cm are fresh juvenile andesite, like that composing pyroclastic-flow deposits of the eruption (Miller and others, this volume); half are lithic cognate andesite and accidental basaltic andesite. The measured densities of 56 projectiles collected at sites 2.9 to 8 km from the vent show a wide range of 1.20 to 2.75 g/cm³ (fig. 4). If

Figure 2. Distribution of August 18, 1992, eruption products, including field of bomb craters. >

a dense-rock equivalent density (ρ_d) of 2.6 g/cm³ (Hall, 1987, table 9) is used for andesite, these clast densities (ρ_c) can be converted into vesicularity percent (V(%)) by the relation $V(\%) = 100(\rho_d - \rho_c)/\rho_d$ (Houghton and Wilson, 1989). The median vesicularity for eight density classes ranges from 0 to 50 percent (fig. 4).

The shapes and densities of gravel-sized clasts reveal something of their history (Houghton and Smith,

1993). Most Crater Peak ballistic clasts are angular and blocky. All clasts denser than 1.9 g/cm³ but slightly vesiculated, have angular edges and blocky shapes (fig. 5), and are very hard under the hammer—clearly lithic. Most juvenile clasts are less dense than 1.8 g/cm³, have microcauliflower surface texture on unbroken faces, are conspicuously vesiculated, and are completely unaltered. Many juvenile clasts have bro-

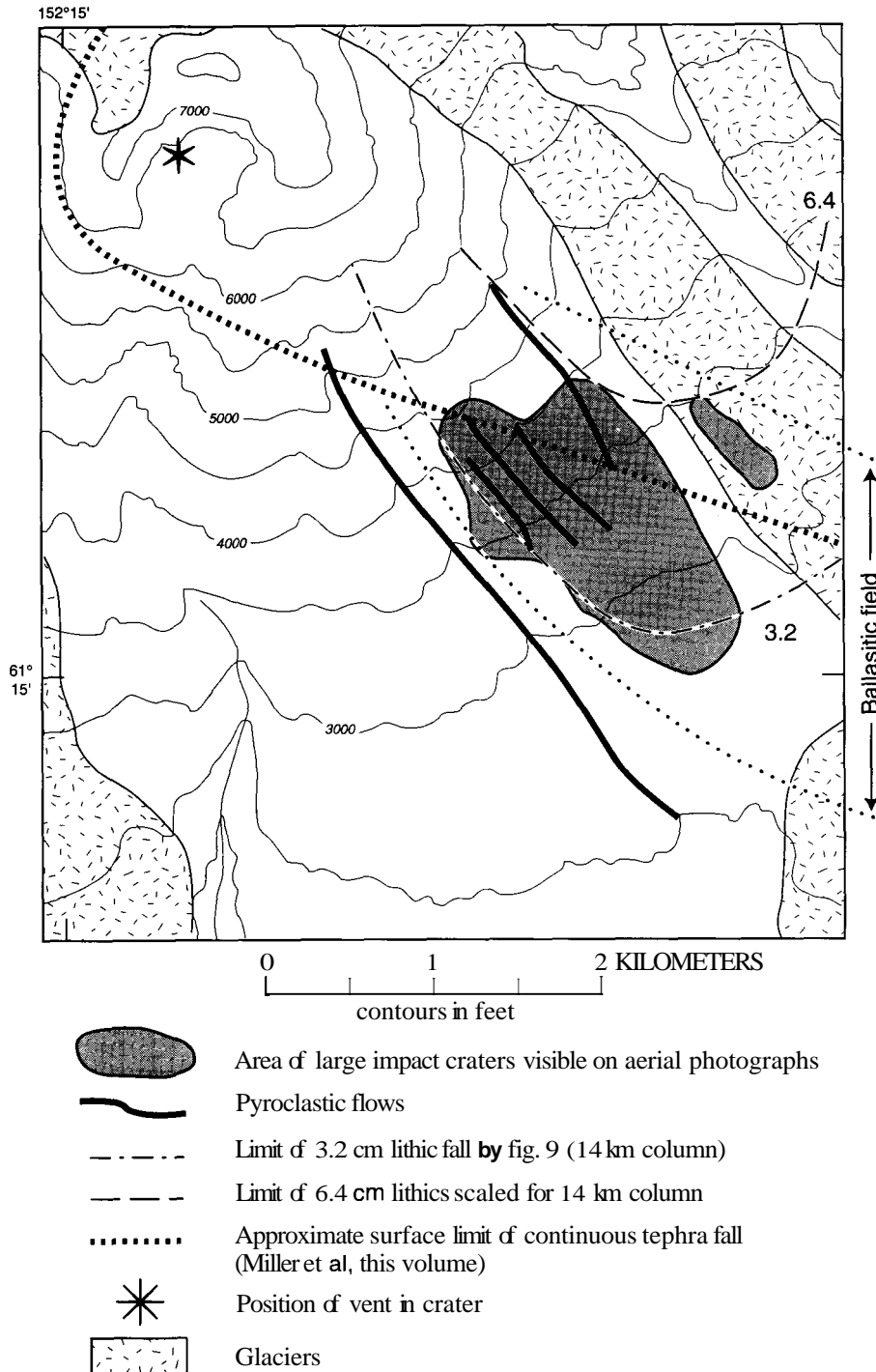




Figure 3. View north of Crater Peak on south flank of Mount Spurr volcano, Alaska. Right (south) margin of field of ballistics thrown by August 18, 1992, eruption approximately shown by dashed line. Field probably extends north beneath area covered by fall and flows of September 1992 eruption. Photograph taken July 27, 1993.

Figure 4. Density distribution of ballistic clasts of August eruption from sites 2.9 to 8.0 km from vent. Calculated vesicularity is also shown (at tops of columns), calculated from an assumed dense-rock-equivalent density of 2.6 g/cm³. Negative vesicularities result from some basaltic-andesite accidental lithic clasts being denser than the assumed 2.6 g/cm³; the area above the line drawn through the two right-hand columns hypothetically distinguishes them.

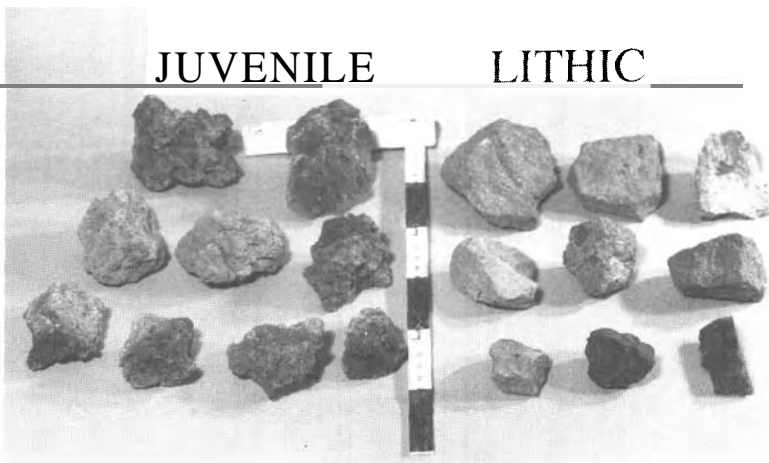
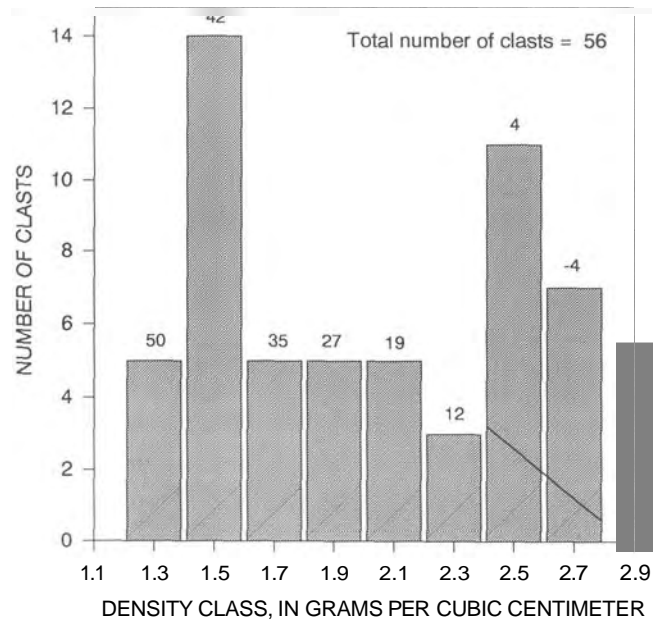


Figure 5. Shapes of small ballistic clasts from the August 18, 1992, eruption of Crater Peak vent, Mount Spurr volcano, Alaska. At center of juvenile group is a small cauliflower bomb, a scarcely vesicular juvenile lithic. The three in lower left are fragments of cauliflower bombs. Bar scale divisions are 5 cm.

ken faces (fig. 5) and show a more vesicular interior and a poorly vesicular exterior. Some juvenile lithic clasts have a more vesicular interior and a scarcely vesicular "lithic" surface. The wide range in density does not vary with throw distance (fig. 6): lithic and juvenile andesite apparently were ejected and traveled together.

Cauliflower-shaped bombs are common among the juvenile clasts (fig. 7). Where best formed, the distinctive texture is nearly identical to bombs photographed from clearly hydromagmatic deposits at Surtsey in Iceland, West Eifel maars in Germany, and Ukinrek maars in Alaska (Lorenz, 1974; Lorenz and Buchel, 1980; Self and others, 1980; Lorenz and Zimanowski, 1984). At Crater Peak, bombs 10 to 15 cm in diameter that were embedded in turf 3 to 4 km downrange

are cauliflowered on top and bottom alike. Because their bottoms were not notably flattened nor their fine texture destroyed, they must have cooled enough to be no longer plastic and deformable upon impact—though they remained hot enough to scorch vegetation beneath them. Many juvenile clasts 2 to 5 cm in diameter are fragments of cauliflower bombs. Typically a third to a half of such a clast is gray to light brownish gray (10YR 611 to 612) and has a micro-cauliflower texture, while the clearly broken faces bounded by sharp angles on other parts of the clast are dark gray to very dark gray (5YR 411 to 3/1). In most such clasts, vesicularity notably decreases from 50 to 30 percent at broken (formerly interior) faces to 15 to 5 percent within 5 mm of the microcauliflowered surficial face.

The size of largest projectiles decreases sharply with throw distances (range) southeast from the vent (fig. 8). Three axes—the maximum, intermediate, and minimum diameters—were measured for many clasts, but because most of the projectiles are subequant to equant, only the intermediate axis is recorded for most of them. The outer limit of large projectiles is fairly sharp: those 40 to 200 cm in intermediate diameter stop at horizontal range 3.2 km, those 20 to 40 cm in diameter stop at 3.6 km, and those 10 to cm in diameter lie throughout the range 2.5 to 8 km. The plot can be interpreted in several ways. First, the steep decrease in large clasts and the long range of small ones may reflect a steeply logarithmic decay of a single population. But second, an outer limit of one population of large (>15 cm) clasts may exist whereas a second population of 1- to 10-cm clasts extends out to at least 8 km.

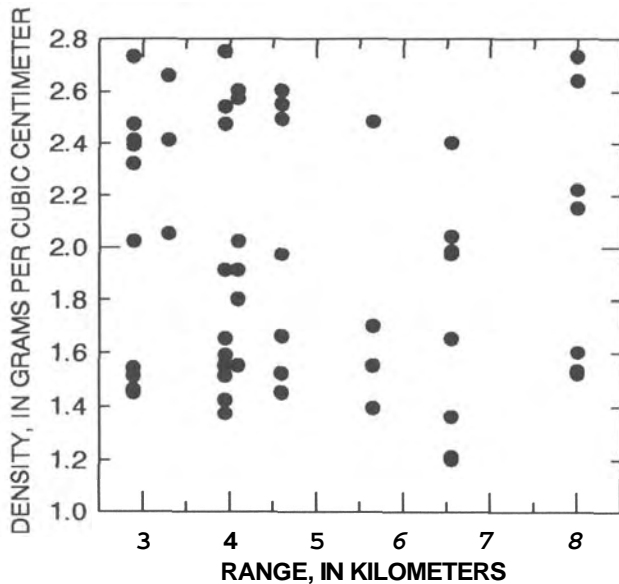
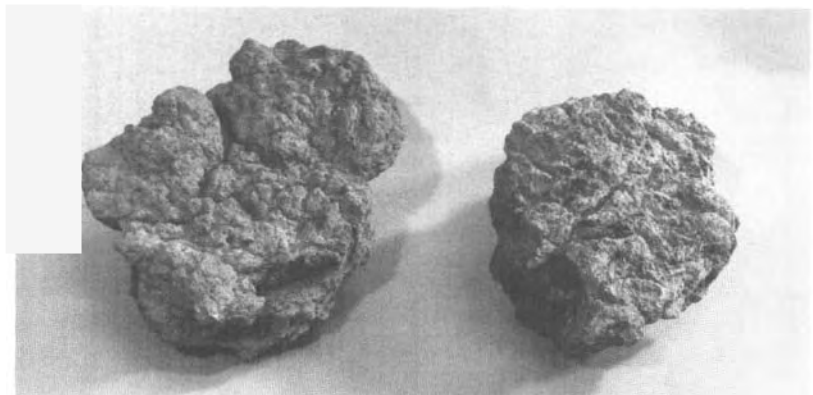


Figure 6. Density of ballistic clasts of August 18, 1992, eruption of Crater Peak vent, Mount Spurr volcano, Alaska, plotted against range of throw.

Figure 7. Cauliflower bombs thrown by August 18, 1992, eruption of Crater Peak vent, Mount Spurr volcano, Alaska. One on left is 12 cm across, that on right 9 cm.



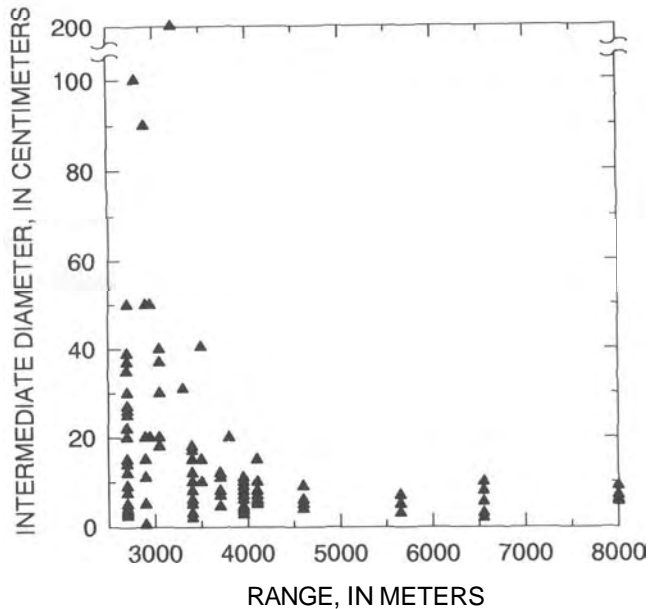


Figure 8. Intermediate projectile diameter plotted as a function of range of throw. Projectiles from August 18, 1992, eruption of Crater Peak vent, Mount Spurr volcano, Alaska.

UNEVEN TEMPERATURES

Many projectiles, both lithic and juvenile, landed in a mat of ground-hugging tundra plants such as caribou moss and scrub blueberry during growth season. Many of the vesicular, clearly juvenile clasts larger than about 10 cm that landed within 4 km of the vent notably scorched the vegetation on which they came to rest—as did juvenile clasts that tumbled off pyroclastic flows and descended into vegetated areas (Miller and others, this volume; Waitt, this volume). Yet beneath lithic ballistic clasts 5 to 50 cm in diameter, identical vegetation was pulverized but scarcely if at all scorched. Among the clasts of the ballistic shower(s), the juvenile ones clearly were much hotter than the lithic ones.

This pattern indicates that the juvenile and lithic clasts did not reach thermal equilibrium before ejection or during flight. The lithic clasts must not have resided at the vent long enough to acquire as high a temperature as the juvenile clasts before explosion(s) ejected them both.

Figure 9. Impact craters of blocks thrown ballistically by 1992 eruptions of Crater Peak vent, Mount Spurr volcano, Alaska. **A**, shattered largish block of August 18, 1992, bomb field; a third of the original clast is the angular block outside crater. **B**, Shattered block of September 17, 1992, that impacted pyroclastic-flow deposit emplaced earlier in same eruption.

IMPACT CRATERS

The largest impact craters range from 3.5 to 5.5 m in diameter and are as deep as 1.5 m. The "target" material is fairly loose, coarse, lithic pyroclastic debris of the 1953 and prehistoric eruptions of Crater Peak, mantled by a thin loam soil and tundra turf (fig. 9). Whereas the largest craters contained bombs as large as 50 cm, most projectile blocks larger than about 35 cm split or shattered upon impact, and parts of them lie outside the crater. When reconstructed, the largest clasts, which lie in and about the largest craters, measure 0.5 to 2 m in intermediate diameter. Craters larger than 3 m in diameter have 2 to 4 rays of ejected material radiating as much as 5 m downrange from the crater rim through 90° to 160° arcs. Clasts as small as 8 cm made impact craters as much as three times their diameter.



RELATION TO WIND, DISTINCTION FROM PROXIMAL FALL

The south limit of fall from the convective vulcanian column (Neal and others, this volume) is uncertain in the area within 10 km of the vent. The south limit of continuous fall is near the apparent north limit of the ballistic field. But within a few kilometers of vent, clasts that fell from the column can be difficult to distinguish from small clasts that moved on ballistic trajectories. During the Mount St. Helens eruptions of 1980, fall from eruption columns occurred through low-level winds oblique to the high-level winds driving the plume. Along the upwind lateral margin in proximal areas, the fall deposit was typically *discontinuous*—pumiceous clasts of sizes between medium pebbles and small cobbles and denser lithic clasts of small- to medium-pebble size (Waitt and others, 1981, figs. 269–273). At Crater Peak (Mount Spurr) on August 18, 1992, low-level winds were *east-north-eastward*, oblique to the upper-level winds carrying the plume east and east-southeast (table 1).

Within the ballistic field 2 to 3.5 km from the vent lie clasts of all sizes from 2 m to 1 cm (fig. 8). The large (>40 cm in diameter) clasts, none of them low-density pumice, are unarguably ballistics, as probably are lithic clasts down to 15 cm or smaller. Yet there is no distinguishable minimum-size limit of bal-

listics detectable in the field. Did the 1- to 10-cm clasts depicted on figure 8 arrive as ballistics or as fall? The discontinuous clasts smaller than 8 cm appear similar to the proximal falls at Mount St. Helens along the upwind lateral margins. Yet at Crater Peak, lithic clasts as small as 8 cm formed impact craters as far as 8 km from the vent in the much finer fall deposits there. Because the larger clasts have higher terminal velocities, they could not have traveled with the finer fall materials without landing first, not last. Therefore the larger clasts that formed small impact craters clearly were ejected later, and thus appear to have been ballistic projectiles. Without additional highly specific field data, distinction between the coarser ballistics and the finer fall is somewhat arbitrary.

Sparks (1986) modeled eruption columns whose diameters typically increase upward as a funnel shape, and Carey and Sparks (1986) analyzed fall from such columns (fig. 10). The highest reach of the Crater Peak eruption column of August 18, 1992, was 14 km (Rose and others, this volume). For a column 14 km high and a downrange wind velocity of 10 m/s, Carey and Sparks's (1986, fig. 14c) model predicts the outer limit of fall of 3.2-cm lithic clasts near the outer edge of the large August 18 impact craters; an extrapolated limit for 6.4-cm clasts lies farther *ventward* of the main ballistic field (fig. 2). Thus by the plume model of Carey and Sparks (1986), lithic clasts only as large

Table 1. Wind data for August 18, 1992, eruption in vicinity of Mount Spurr volcano, Alaska.

[A. Projected winds beginning 7:00 p.m. August 18, 1992]

Altitude (ft)	Azimuth toward (degree)	Wind velocity (m/s)	Wind toward azimuth 135 (m/s)
5,000	17	4.8	-2.3
10,000	71	5.2	2.7
18,000	72	11.1	5.0
23,000	96	11.1	8.7
30,000	104	14.7	12.7

Source: National Weather Service

[B. Balloon sounding above Anchorage at 4:00 p.m. August 18, 1992]

Altitude (ft)	Azimuth toward (degree)	Wind velocity (m/s)	Wind toward azimuth 135 (m/s)
6,000	350	6.2	-3.5
8,000	30	5.1	-1.3
12,000	50	7.2	0.6
16,000	70	9.3	3.9
20,000	85	10.8	6.9
25,000	115	15.9	15.0
30,000	130	22.1	22.0

Source: National Weather Service

as 3 to 6 cm should have fallen as tephra within the area of the August 18, 1992, Crater Peak ballistic field. Were column height somewhat higher or winds higher than reported, somewhat larger clasts could have fallen in the shaded area shown in figure 2. By stretching the envelope of uncertainty, one can imagine lithic clasts as large as 8 cm being possibly related to airfall near the southeast part of the shaded area, but it doesn't help to explain larger clasts, which therefore must be ballistics.

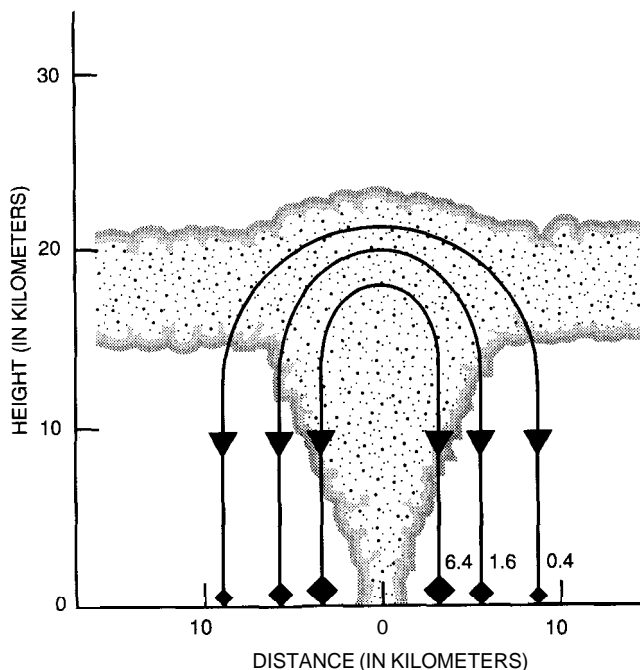


Figure 10. Fall of lithic (density = 2.5 g/cm³) clasts from modeled column roughly 1.5 times the height of the maximum reported for the August 18, 1992, eruption of Crater Peak, Mount Spurr volcano, Alaska eruption (illustration from Carey and Sparks, 1986, fig. 6). Scale is true (no vertical exaggeration). Upward flare of model, about 23° from the vertical, is about that shown by Crater Peak eruption photographs of August 18, 1992. Symbols show theoretical outer limit of lithic clasts 6.4, 1.6, and 0.4 cm in diameter. Outer limit of 6.4-cm lithic clasts is 3.3 km from plume axis, the limit of 1.6-cm clasts 5.5 km. The modeled column is much higher than the Crater Peak column, thus the distance of lateral fall from plume axis is maximum-limiting case.

RECONSTRUCTED VELOCITIES OF BALLISTIC PROJECTILES

Some elements of the trajectory of a ballistic projectile can be inferred from its impact point, including minimum ejection velocity. From minimum velocity of an ejected block, vent pressure required to expel the block can be calculated within very broad limits and with considerable uncertainties.

METHOD

Wilson (1972) reconstructed volcanic-ballistic trajectories utilizing data on drag forces on cylinder-shaped projectiles. To reach a given distance from the vent, a small projectile (say 10 cm) requires a far higher launch velocity than does a large (1 m) one, because for a small particle the ratio of surface area to mass is much higher, thus drag per unit mass much higher.

The velocity required to eject blocks to the distances observed at Crater Peak is estimated by computing ballistic trajectories for blocks of known properties using an algorithm outlined in Wilson (1972). Components of velocity (v) in the horizontal (x) and vertical (z) directions are given by:

$$v_x = v \cos \theta \quad (1a)$$

$$v_z = v \sin \theta \quad (1b)$$

where θ is trajectory angle measured from the horizontal. At any given point along a particle's trajectory, the rates of change of v_x and v_z are given by:

$$\frac{dv_x}{dt} = \frac{-v_x \rho_a v A C_d}{2m} \quad (2a)$$

$$\frac{dv_z}{dt} = \frac{-v_z \rho_a v A C_d}{2m} - g \quad (2b)$$

where ρ_a is air density, A is cross-sectional area of the block, C_d is drag coefficient on the block, m is the block's mass, g is gravitational acceleration, and t is time. These equations are identical to equations 3 and 4 in Wilson (1972), though variables have been rearranged and different symbols are used to designate them. The variables A and m depend on the shape and size of the block, assumed in this case to be spherical (that is, $A = \pi r^2$ and $m = (4/3)\pi r^3 \rho_r$), with block radius (r) equal to the intermediate measured block semidiameter, and rock density (ρ_r) equal to 2.5 g/cm³. Air density (ρ_a) varies with height and was recalculated at each point in the trajectory using the following equation, which is a best-fit curve through published altitude-density data (Ahrens, 1991, p. 546):

$$\rho_a = .0012232 - 1.1389 \times 10^{-7} (z_0 + z) + 3.3036 \times 10^{-12} (z_0 + z)^2 \quad (3)$$

where z in this case is the vertical position above the vent, and z_0 is the altitude of the vent above sea level (air densities in g/cm^3 , altitude in meters).

Equations 2 above were integrated throughout the trajectory using a fourth-order Runge-Kutta method, as were those of Wilson (1972). This algorithm was made more versatile by incorporating corrections for tailwind velocity (w) downrange from the crater, and an altitude difference (ξ) between the launch and landing sites (ξ is <0 for sites that are lower than launch site, like all calculated herein). The correction for altitude difference was included by simply calculating the trajectory until the vertical position (z) of the block reached its landing elevation (z_f), which generally differs from launch altitude ($z=0$). The wind correction was made by substituting $(v_x - w)$ for v_x in equation 2a, and $\sqrt{v_z^2 + (v_x - w)^2}$ for v in equations 2a and 2b.

DRAG

Drag coefficient C_d influences the final range of the blocks enormously but is poorly constrained for use with volcanic ballistics, for the experimental data show that drag on a projectile varies greatly with its shape, orientation, and roughness. Experimental results (for example, Hoerner, 1965) indicate that C_d for variously shaped objects traveling through fluids varies with two dimensionless numbers that indicate flow regime: Reynolds number (Re) and Mach number (M). Reynolds number relates the relative importance of viscous versus inertial forces in the fluid by the relation (for external flow) $Re = vdp/\eta$, where v is particle velocity, d is particle diameter, ρ is fluid

density, and η is fluid viscosity ("fluid" here being air). The range of particle sizes and calculated velocities give Reynolds numbers (Re) greater than or equal to 4×10^5 . Drag coefficient C_d for smooth spheres is 0.06 at Re of 4×10^5 and rises gradually to 0.2 at Re greater than about 1×10^7 (fig. 11) (Hoerner, 1965, figs. 3-10, 3-11; Achenbach, 1972, fig. 4).

Most authors analyzing volcanic ballistics have used high drag coefficients. In experiments on falling pyroclasts, Walker and others (1971) showed that for terminal velocities of small particles falling at low velocities (hence low Reynolds numbers), the relatively high drag coefficients for cylinders were more appropriate than the lower coefficients for spheres. Thus Wilson (1972) and Fagents and Wilson (1993) assumed that C_d measured for cylinders applied to irregularly shaped blocks. For such objects several other authors have also assumed rather high values of C_d , usually around 1.0 and no lower than 0.7 (Minakami, 1942; Fudali and Melson, 1972; Steinberg and Lorenz, 1983; Self and others, 1980; Wilson, 1980; Mastin, 1991).

Mach number ($M \equiv v/c$) gives the speed of the object (v) relative to the fluid's sonic velocity (c). For air under ambient conditions, the sonic velocity is about 350 m/s. As long as objects are traveling at speeds less than about 70 percent of the sonic velocity (that is, less than about 250 m/s), C_d varies with Reynolds number only. But at Mach numbers above about 0.7, the production of sound waves (and shock waves when $M \geq 1$) dissipates energy. Drag coefficients rise dramatically for Mach numbers in the range 0.7 to 1.5 and stabilize for Mach numbers above 1.5 (fig. 12).

To calculate ballistic trajectories for the irregularly shaped blocks at Crater Peak, we assumed drag coefficients for spheres (which have low drag) and

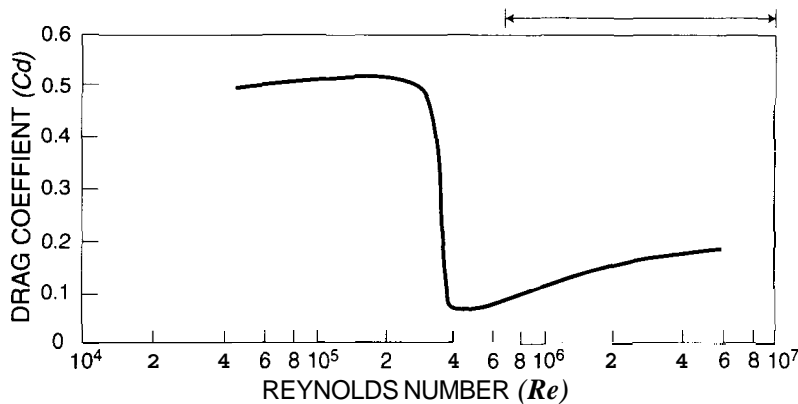


Figure 11. Low drag coefficients for smooth spheres at very high Reynolds numbers (from Achenbach, 1972, fig. 4). Bar with arrowheads shows range of Reynolds numbers calculated from initial velocities computed for ballistic clasts from the 1992 eruptions of Crater Peak, Mount Spurr volcano, Alaska.

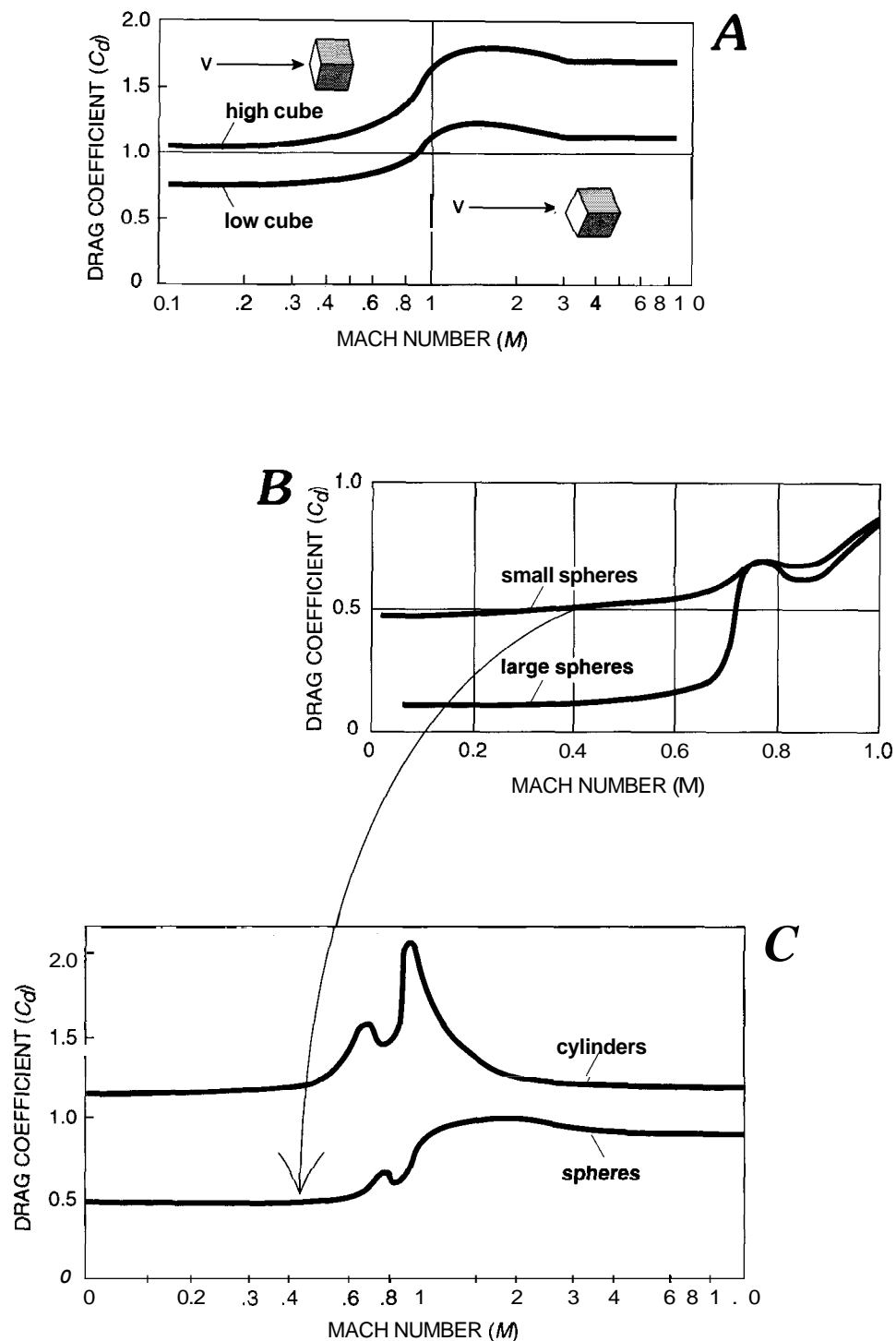


Figure 12. Drag coefficients for (A) cubes at transonic velocities, (B) spheres at velocities approaching sonic, and (C) cylinders (top curve) and spheres (lower curve) at transonic velocities. Top curve in (A) represents drag coefficients for cubes oriented with one face perpendicular to the direction of motion. Bottom curve represents drag for cubes oriented with the vertex between three faces at the leading edge of the cube. Top curve in (B) represents drag coefficients for small spheres at Reynolds numbers below the critical transition ($Re \sim 2 \times 10^5$), whereas the lower curve represents drag coefficients for large spheres at Reynolds numbers above the critical transition. The ballistic model calculates Reynolds number at each point in the trajectory and uses the drag appropriate at the calculated Reynolds and Mach numbers (for all blocks analyzed in this study, the appropriate drag coefficient is represented by the large-sphere curve). Calculations for supersonic velocities used drag coefficients for spheres illustrated in (C). Modified from Hoerner (1965).

for cubes (with high drag) (table 2). At each point in the trajectory the Mach number (taken from fig. 12) was used for the next calculation. Results from this program using some typical input parameters are shown in figure 13 for a launch angle of 45° .

We back-calculate initial velocities for the largest one or two projectiles from each small sampled area. Altitude of impact site (Z_{final} or Z_f) was measured in the field by altimeter and plotted on a topographic map, from which range (x_f) was read. We assume a lithic particle density of 2.5 g/cm^3 and launch angles between 30° and 35° —the most efficient launch angles calculated by the program under the conditions of range less than 4 km and with impact altitude far below launch altitude. We assume downrange windspeed of 0 m/s ; calculations with the highest permissible windspeed (10 m/s) do not substantially affect results.

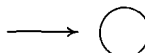
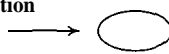

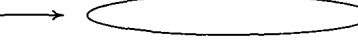
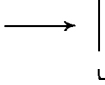
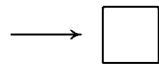
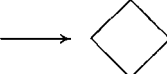
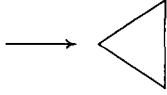

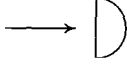
Our results for ballistic clasts thrown by Crater Peak are shown by table 3, calculated using values of C_d measured for spheres and cubes. At the very high Reynolds numbers ($Re > 4 \times 10^5$) typical for Mount Spurr

ballistics, C_d for smooth spheres can be as low as 0.06 (fig. 11) but for very rough objects may be much higher.

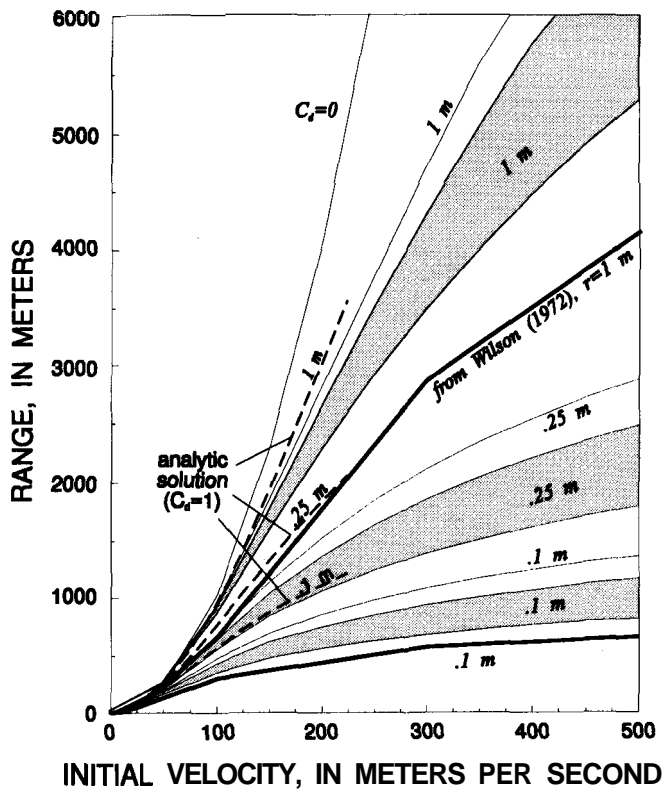
For comparison to the Mount Spurr data is a synopsis of ballistics thrown by other eruptions, calculated with a constant high drag coefficient ($C_d=1$) used by investigators of those eruptions. At drag coefficient $C_d=1$ (table 3, col. 8), our calculated initial velocities at Ukinrek maars and Inyo Craters—where ballistic clasts are fairly large and maximum range only about 700 m—are near the values 85 to 100 m/s reported by Self and others (1980) and Mastin (1991) respectively. The calculated initial velocities for the large ballistics at moderate to long distance at Asama in 1938, Arenal in 1968, and Ngauruhoe in 1975, (195–322 m/s) are also well below sonic velocities, more so than originally reported (Minakami, 1942; Fudali and Melson, 1972; Nairn, 1976).

If we use a constant $C_d=1$ at Crater Peak (Mount Spurr), subsonic velocities are given only by the largest (2 m) clast thrown to moderate range, whose calculated v_i is 183 m/s (table 3, col. 8). The only other

Table 2. Drag coefficients for three-dimensional shapes.

Shape	Laminar flow	Turbulent flow
Sphere 	0.47	0.10
Ellipsoidal body with circular cross section		
2 : 1 	0.27	0.06
4 : 1 	0.20	0.06
8 : 1 	0.25	0.13
Disk 		1.17
Cube 		1.05
		0.80
60° cone 		0.49
Solid hemisphere:		
Convex surface to flow 		0.38
Flat face to flow 		1.17

Adapted from Mironer (1979, table 8.2)



clasts yielding subsonic (barely) initial velocities are 50 cm or more in diameter. Ballistics 37 to 39 cm in diameter even in the *nearest* part of the sampled range (2.7 km) yield much higher supersonic velocities (>400 m/s). Calculated velocities above 700 m/s (Mach number ≈ 2) for projectiles of smaller size and (or) those thrown to greater range seem unreasonably high.

If now these clasts are calculated using a variable drag coefficient as low as $C_d=0.06$ —the values for smooth spheres when Re exceeds 4×10^5 (fig. 11)—ballistic clasts with diameters as small as 15 cm have

Figure 13. Initial velocity of blocks ejected plotted as a function of range assuming wind velocity $w=0$ m/s, impact altitude below vent altitude $\xi=0$ m, density of projectiles $\rho=2.5$ g/cm³, and the initial trajectory angle is 45° from horizontal. Shaded regions represent results using drag coefficients for cubes, thin solid lines represent results using drag coefficients for spheres. Heavy solid lines are values from Wilson (1972) based on drag coefficients for cylinders. Dashed lines show values from the approximate analytical solution of Minakami (1942) (see also Self and others, 1980; Mastin, 1991) that assumes a constant drag coefficient $C_d = 1$.

Table 3. Ballistics of August 1992 eruption of Crater Peak, Alaska.

[Vent altitude, 1,952 m. C_d , drag coefficient; Re , Reynolds number; M , Mach number]

Station No. 1993	Range (m)	Altitude (m)	Altitude difference (m)	Azimuth (degree)	Diameter (cm)	INITIAL VELOCITY			
						Vacuum $C_d=0$ (m/s)	Fixed C_d $C_d=1$ (m/s)	C_d variable with Re and M	
								Sphere (m/s)	Cube (m/s)
.01	2700	976	-976	140	37	140	432	156	342
.02	2700	976	-976	140	39	140	398	156	319
.02	2700	976	-976	140	25	140	1025	165	761
.03	2700	968	-984	140	9	140	Infinite	194	Infinite
.04	2900	961	-991	133	50	145	331	160	277
.05	2950	930	-1022	133	50	146	340	162	283
.06	2950	930	-1022	133	20	146	3400	184	2411
.08	3200	891	-1061	132	200	154	183	157	175
.09	3400	857	-1095	133	17	159	Infinite	219	Infinite
.10	3400	851	-1101	134	18	159	Infinite	216	Infinite
.11	3300	866	-1086	134	31	156	914	188	839
.12	3500	836	-1116	137	40.5	162	672	189	534
.12	3500	836	-1116	137	15	162	Infinite	245	Infinite
.13	3700	817	-1135	138	11	167	Infinite	604	Infinite
.14	3800	787	-1165	139	20	169	Infinite	248	Infinite
.15	4100	790	-1162	140	15	177	Infinite	582	Infinite
.19	3950	747	-1205	137	11	172	Infinite	936	Infinite
.20	6550	628	-1324	134	10	231	Infinite	Infinite	Infinite
.24	8000	686	-1266	121	9	262	Infinite	Infinite	Infinite
Asama 1938	3500		-1100		100		266	(Minakami, 1942)	
Ngauruhoe	2800		-980		80		237	(Nairn, 1976)	
Arenal	5000		-500		200		291	(Fudali and Melson, 1972)	
Ukinrek	700		0		200		87	(Self and others, 1980)	
Inyo	700		40		40		108	(Mastin, 1991)	

subsonic velocities (table 3, col. 9). The larger projectiles (intermediate diameters between 200 and 17 cm) thrown downrange 2.7 to 3.5 km give reconstructed initial velocities between 156 and 248 m/s. For smooth spheres the variable C_d of table 3, column 9 is low throughout most or all of a clast's range, except where required initial velocity exceeds Mach number 0.7, which triggers the use of higher drag coefficients taken from figure 12. Under the drag assumptions for smooth spheres, implied vent velocities for the particles of 18 cm and larger thrown from Crater Peak during its August eruption were between 160 and 250 m/s.

Figure 14 illustrates the highly variable drag for a sphere initially shot at 400 m/s. During the initial part of its flight, drag coefficient is about 0.85 and falls to 0.65 in the first one-sixth of its flight. Then as Mach number drops below 0.7, drag falls off rapidly to 0.2. From there it drops even lower as veloc-

ity reaches a minimum at the top of the trajectory, and then rises back to about 0.2 as velocity increases on the downward leg of the trajectory.

Volcanic particles are not spheres and many have angular faces. Wind-tunnel drag data are readily available (Hoerner, 1965) for cubes. If we test the Crater Peak ballistics with these drag coefficients for cubes, all but the largest block would have required initial velocities above 400 m/s. Many of those exceed even maximum theoretical velocities for eruptions under nearly all reasonable initial pressure conditions (about 2000 m/s, Mastin, 1995). Of the many apparently ballistic projectiles smaller than 18 cm in diameter that landed downrange 2.7 to 8.0 km from the vent (fig. 8), implied initial velocities are 500, 1000, 2000 m/s and higher. The more the calculated values for initial velocity exceed 400 m/s, the less believable they are.

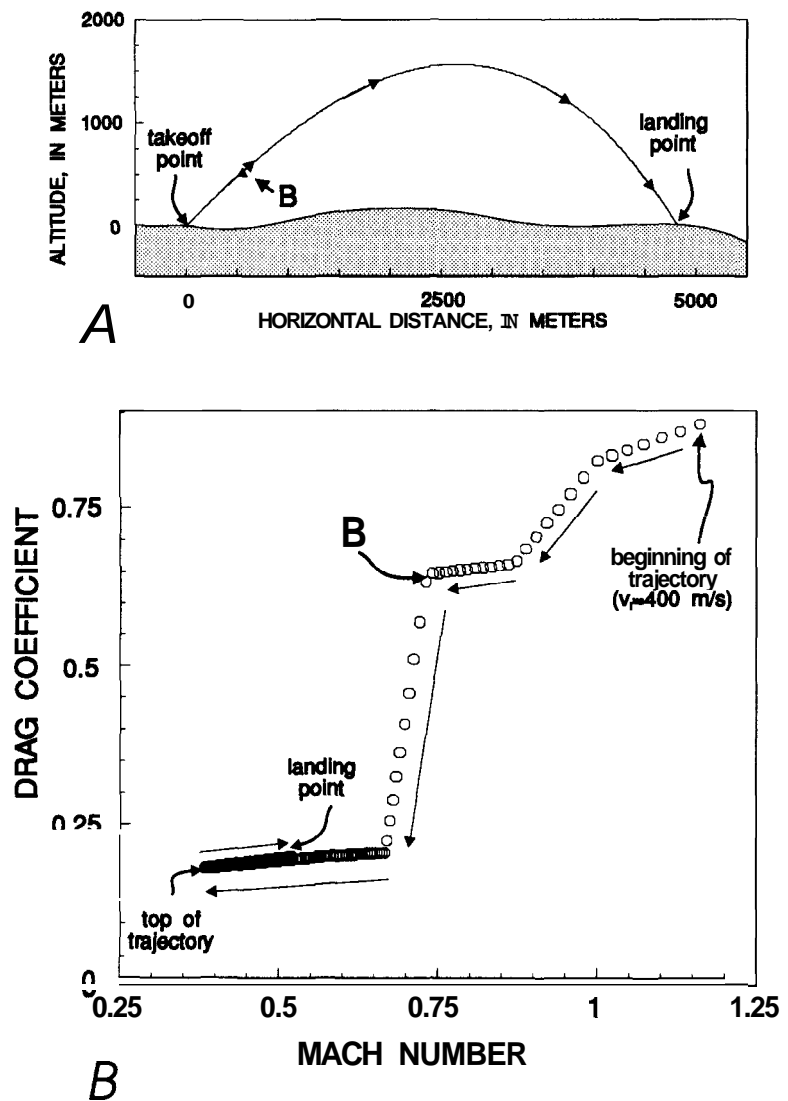


Figure 14. Successively, sharply lower drag coefficients of typical ballistic block thrown from Crater Peak whose velocity is initially supersonic. A, Block's vertical trajectory during flight. B, Change in drag coefficient during flight.

DISCUSSION

Most or all students of volcanic ballistics have followed Walker and others (1971) in assuming high drag coefficients (as for cylinders) in calculating trajectories of volcanic ballistics, and no other experiments have appeared to test that analysis. But calculations using such high drag give impossibly high initial velocities for the smaller of the Crater Peak clasts that are clearly ballistics.

Drag data on cubes compiled by Hoerner (1965) also entails fairly high drag coefficients (fig. 12A). High drag in the computations yields the high initial velocities for a clast even of moderate size (say, 20–40 cm) to be thrown to moderate range (say, 2.5 to 3.5 km). These results are then compounded where Mach numbers exceed 0.6, above which drag further increases significantly (fig. 12B,C).

Velocities of 100 to 250 m/s of clasts 0.1 to 1.0 m in diameter generate Reynolds numbers between about 7×10^6 and 1×10^7 . This is the range of very high Reynolds numbers explored by Achenbach (1972) for smooth spheres, whose drag coefficients he measured to be very low—below 0.2, even as low as 0.06 (fig. 11). Terminal velocities exceeding 40 m/s of ballistics larger than 5 cm in diameter keep them from "mov-

ing leftward" on figure 11 below Reynolds numbers smaller than 5×10^6 and into a range of much higher drag coefficients, even toward the end of their flight. If the flight of a particle occurs mostly or entirely within this envelope of low drag, 10- to 40-cm particles thrown even to range 4 to 8 km would require initial velocities far below sonic velocity (table 3, col. 9). We sense that the much lower drag coefficients permitted by wind-tunnel data on spheres where Reynolds numbers are greater than 4×10^6 is the key to unlock the enigma of far-traveled small ballistics.

While drag coefficients for very rough volcanic particles generally exceed those for smooth spheres, there may be compensating effects. For instance, slight roughening of a smooth sphere increases turbulence in the boundary layer and causes the wake to be much smaller (fig. 15); thus drag is reduced. Photographs illustrating this principle are shown in many textbooks on fluid mechanics (Rouse, 1946, plate 16; Mironer, 1979, fig. 8.19; White, 1979, fig. 7.14). A golf ball "roughened" by inverse topography ("dimples") travels farther than a smooth one (Jorgensen, 1993, p. 62–64).

The surfaces of volcanic ballistics may be irregular in shape, but few resemble the least aerodynamic geometric solid (cube) tested in wind tunnels

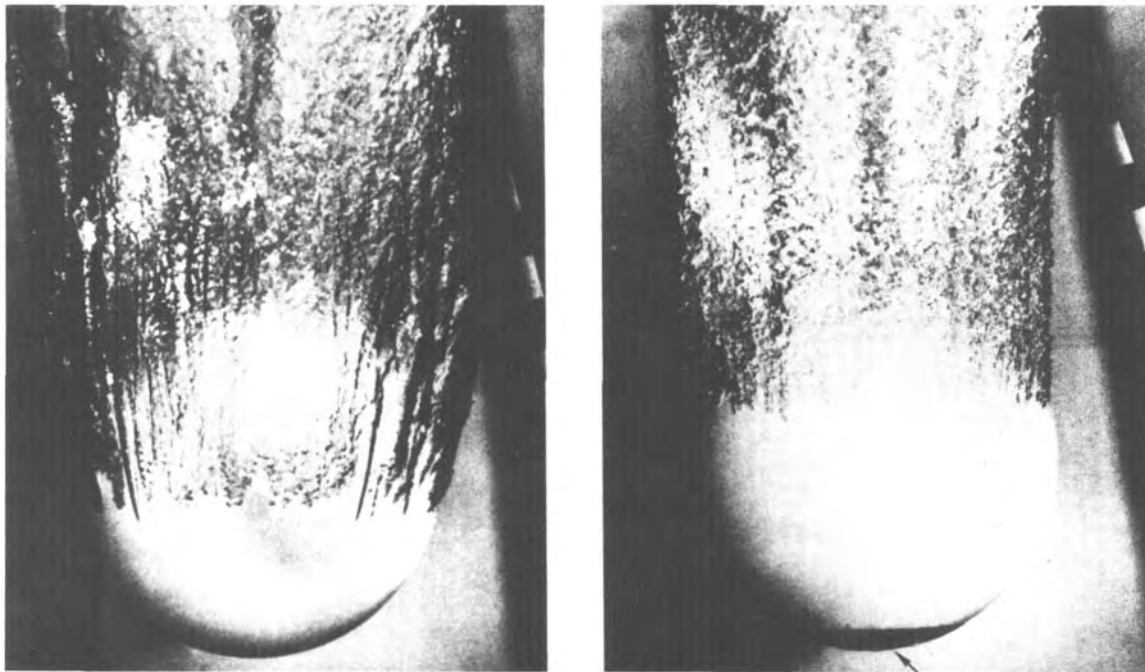


Figure 15. Bowling ball in two experiments generating similar Reynolds numbers. The roughened surface of ball on right (sandpaper patch at base [arrow] causes "premature" boundary-layer turbulence and consequent decrease in area of wake in lee of sphere, compared with that of smooth ball. The smaller wake decreases the relative vacuum behind the object that exerts a small backward force on it, and hence decreases total drag. From Waugh and Stubstab (1973, fig. 15.6).

(table 2). Until actual volcanic ballistics are tested in wind tunnels, one can only infer that drag coefficient will be somewhere between about 0.06 and 1.5 at substantially subsonic velocities. If the lower end of this enormous range proves at all close to reality, the evidently "impossible" great range achieved by some smallish ballistic particles will be partly explained.

FACTORS BESIDES DRAG

Other factors besides a cannonlike ejection into a continuous air-drag environment must influence the great distance traveled by many of the smaller blocks. These other factors could include: (1) much higher tailwinds than assumed in the model, (2) convective lift during flight, (3) large blocks traveling mostly intact but then disaggregating before landing, (4) smaller blocks drawn behind larger blocks or ejected as aggregates with other blocks and thus collectively subject to less drag than imposed on blocks separately, and (5) shock waves and other forward air movement attending ejection of blocks, which reduce air drag during the first part of the trajectory. These five factors are examined below.

Using a range of hypothetical tailwind velocities, we calculate initial ejection velocities for the 40.5-cm block thrown 3.5 km from the vent (table 4). Even with a low drag coefficient appropriate for smooth spheres and the lowest appropriate for cubes, tailwind velocities exceeding 35 m/s are required throughout the trajectory to bring ejection velocities within the less than 400 m/s range of velocities previously observed. With the higher drag coefficients for cubes, required tailwind velocities would be about 60 m/s. Such hypothetical wind speeds are 5 to 30 times those shown by the NOAA data for August 18, 1992, (table 1).

Table 4. Hypothetical effect of tailwind in carrying blocks to greater distance.

[Example of a 40.5-cm-diameter block thrown to range 3,500 m and landing 1,116 m below vent altitude]

Wind Velocity (m/s)	Initial Velocity (m/s)
0	1200
10	770
20	575
40	330
60	210
80	160

Convective lift cannot explain the distance traveled by the larger blocks. The terminal velocity of blocks 40 cm in diameter is 100 to 300 m/s in air (depending on drag coefficient chosen) as calculated from a standard equation (Mironer, 1979, p. 277). Only updrafts a large fraction of terminal velocity would greatly lengthen a block's trajectory. Convective updrafts of tens of meters per second or more occur in sustained plinian eruptive columns (Woods, 1988), but it is unlikely that transient bursts such as at Crater Peak could sustain such drafts. Yet clasts smaller than 5 cm diameter, whose terminal velocities are less than 50 m/s, could be somewhat affected by small updrafts. Perhaps this factor, operating during the subplinian phase of the first 3 hours of the eruption (Neal and others, this volume) especially in an upward-funneling column as analyzed by Sparks (1986) and by Carey and Sparks (1986), could explain the many lithic and juvenile clasts smaller than 5 cm scattered throughout the ballistic range as elements of fall. Yet because most of the ballistics apparently were ejected near the end of the eruption, some traveling as far as 8 km from the vent even after the subplinian fall had ended, sustained updrafts seem unimportant for many of the small ballistic clasts.

If larger blocks somehow disaggregated in flight just before landing, the ballistic blocks should lie in clusters of broken fragments of like lithology. Such a clustering was nowhere decipherable, except purely hypothetically if applied to juvenile clasts scattered throughout the impact area. The many fragments of cauliflower bombs seemed randomly and widely dispersed, as though they were shattered upon explosion at the vent, not near the end of their flightpath. Some juvenile clasts are completely rimmed with quenched margins (figs. 5, 6) and clearly did not fragment in the air or on impact. In-flight fragmentation therefore does not help explain the large distances traveled by many of the blocks.

Numerous images of explosive "cocktail plumes" captured on movie film, video, and photographs (for examples, Williams and McBirney, 1979, p. 251; G. Rosenquist in Voight, 1981, p. 75-76) show each fingerlike projection to be led by a large block in whose wake trails a cloud of smaller debris. At Crater Peak this could help explain many small blocks within the 3.5-km-range limit of large blocks. Yet the smaller blocks extend much farther (fig. 8), and they are about as plentiful just beyond the limit of large blocks as just inside that limit. Thus smaller fragments drawn behind large ones cannot be important in the outer half of the August ballistic field.

Forward air movement attending the whole complex process of ejection has been suggested to aid the flight of ballistics (Wilson, 1980), a concept supported by visual observation of shock waves accom-

panying explosive eruptions (Nairn and Self, 1978; Ishihara, 1985). Fagents and Wilson (1993) included this effect in their ballistic analysis by considering that the blocks were ejected within an envelope of air whose velocity (initially the same as that of the blocks) decayed exponentially with time.

DISCUSSION

Convective uplift helps explain many small apparent ballistics lying generally outside the continuous-airfall field as clasts that dropped from a funnel-shaped eruption column as shown by Carey and Sparks (1986, figs. 3, 13). Several researchers think that gas streaming from the vent could account for small particles thrown to the same or even greater range as large particles (Lorenz, 1970; Self and others, 1980; Mastin, 1991). Fagents and Wilson (1993) offer a numerical modification of Wilson (1972) that takes into account a gas-expansion phase 25 to 150 m outward from the vent, which reduces but does not eliminate the unreasonably high initial velocities that calculations for smaller particles yield. Further analysis of a gas-expansion phase during the Crater Peak ballistic explosions and of drag coefficients is in progress (L.G. Mastin and R.B. Waitt, unpub. data).

HYDROVOLCANIC NATURE OF EXPLOSIONS

Violent explosions caused by rapid intermixing of molten material and water have been analyzed in industrial and volcanic settings (Colgate and Sigurdsson, 1973; Peckover and others, 1973; Wohletz, 1983; Wohletz and McQueen, 1984). Swift interaction of magma with external water could help explain the transiently high pressure generated at apparently shallow depths near the end of the August eruption of Crater Peak. The August eruption lasted about 4 hours. As magmatic vent pressure waned, ground water from the cone may have poured into the vent along with ejecta fallback and talus from the overhanging northwest crater wall. Mixing of hot rock and water in the vent, contained beneath collapsing crater walls and slumping talus, could fuel hydroexplosions. Most of the ballistic blocks from Crater Peak are angular, blocky lithic clasts and cauliflower bombs (mostly fragmented cauliflower bombs). Vesicularity among juvenile clasts is only low to moderate (generally <50 percent), and the range in vesicularity is high. These characteristics resemble hydromagmatic deposits elsewhere and contrast with strombolian deposits having higher vesicularity and fluidal external shapes (Lorenz and Biichel, 1980; Self and others, 1980; Lorenz and Zimanowski, 1984; Houghton and Hackett, 1984;

Houghton and Schmincke, 1989; Houghton and Nairn, 1991). Thus the explosions late in the August eruption appear to have been propelled by hydromagmatic processes rather than by vesiculation of magma.

Eruptions of some stratovolcanoes have evolved from magmatic to hydromagmatic as an eruption wanes. As the Vesuvian A.D. 79 magmatic eruption dwindled, interaction of magma with external water produced the final surge beds (Sheridan and others, 1981; Sigurdsson and others, 1985). Increased interaction with water also occurred near the end of many other Vesuvian eruptions from Pleistocene to recent (Sheridan and others, 1981; Rosi and Santacroce, 1983; Rosi and others, 1993; Bertagini and others, 1991).

HORIZONTALLY CURVING TRAJECTORIES

Many ballistic projectiles at Crater Peak are embedded in the downrange side of the impact crater, or they shattered and the fragments spread downrange from the crater, which indicate the projectiles arrived at distinct angles to the vertical. Most impact craters are elongate and have an asymmetric ejecta rim. The largest craters have ejecta rays radiating on one side. Both phenomena register the azimuth of the block's impact.

In the accessible right-marginal part of the August 1992 ballistic field investigated, some impacts point directly away from the Crater Peak vent on an azimuth of 135° , yet most of them along this general azimuth point more southward than in a straight line from the vent (fig. 16). A typical southward deviation is 20° to 40° south, the maximum 67° . In this downrange right side of the ballistic field, the deviation is systematically southward; no trajectory has the opposite displacement from a straight line. The southward tendency at the end of the ballistic trajectories was despite the ambient wind toward the east-southeast (toward about azimuth 115°), which tended to straighten out (that is, shift eastward) any south-curving trajectories. The angular deviation from a straight-line trajectory seems to be largely independent of a projectile's diameter.

A pitched baseball or softball will always curve in the direction of a sharply applied spin. This phenomenon, known as the "Magnus effect," has been variously analyzed by Briggs (1959) and Adair (1990), among others. The systematic map-view pattern at Crater Peak—of which we have found no other example in the literature on volcanic ballistics—suggests that many of these clasts had a notable angular velocity about strongly vertical axes. The deviant clasts that curved systematically rightward (viewed from above), if caused by spinning, would have spun clockwise.

In several movies and videos showing typical low-energy strombolian-type explosions, the clasts do not spin much, certainly less than 1 rev/s. If spinning is the cause of deviations in the horizontal component of trajectory of the Crater Peak ballistics, it must be a phenomenon induced by high-energy ejection.

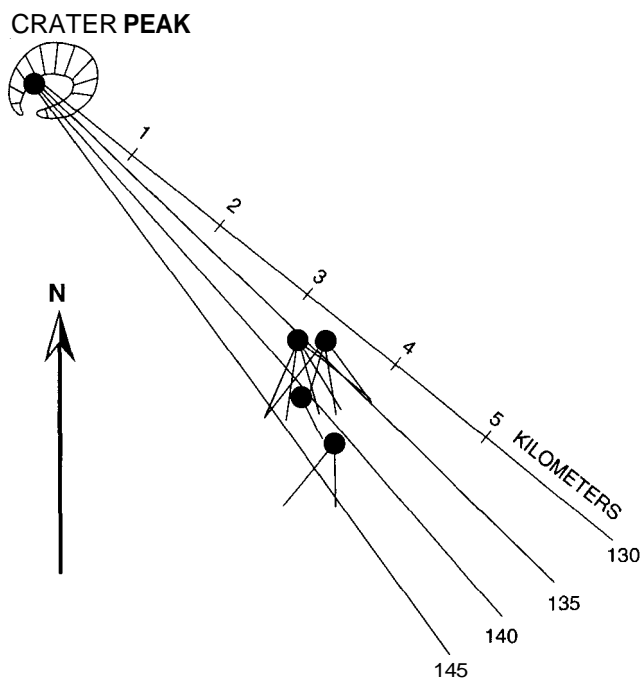


Figure 16. Azimuths of projectiles arriving at right margin bomb field of August 18, 1992, eruption of Crater Peak vent, Mount Spurr volcano, Alaska.

REFERENCES CITED

- Achenbach, E., 1972, Experiments on the flow past spheres at very high Reynolds numbers: *Journal of Fluid Mechanics*, v. 54, p. 565–575.
- Adair, R.K., 1990, *The physics of baseball*: New York, Harper Row, 110 p.
- Ahrens, C.D., 1991, *Meteorology Today*, 4th ed.: St. Paul, Minn, West Publishing Co., 577 p.
- Bertagini, A., Landi, P., Santacroce, R., and Sbrana, A., 1991, The 1906 eruption of Vesuvius—from magmatic to phreatomagmatic activity through the flashing of a shallow depth hydrothermal system: *Bulletin of Volcanology*, v. 53, p. 517–532.
- Briggs, L.J., 1959, Effect of spin and speed on the lateral deflection (curve) of a baseball; and the Magnus effect for smooth spheres: *American Journal of Physics*, v. 27, p. 589–596.
- Carey, S., and Sparks, R.J.S., 1986, Quantitative models of the fall-out and dispersal of tephra from volcanic eruption columns: *Bulletin of Volcanology*, v. 48, p. 109–125.
- Colgate, S.A., and Sigurgeirsson, T., 1973, Dynamic mixing of water and lava: *Nature*, v. 244, p. 552–555.
- Fagents, S.A., and Wilson, L., 1993, Explosive volcanic eruptions—VII. The ranges of pyroclasts ejected in transient volcanic explosions: *Geophysical Journal International*, v. 113, 359–370.
- Fudali, R.F., and Melson, W.G., 1972, Ejecta velocities, magma chamber pressure and kinetic energy associated with the 1968 eruption of Arenal volcano: *Bulletin Volcanologique*, v. 35 (2), p. 383–401.
- Hall, A., 1987, *Igneous petrology*: New York, John Wiley & Sons, 573 p.
- Hoerner, S.F., 1965, *Fluid Dynamic Drag*: Vancouver, Wash., (published by author), 450 p.
- Houghton, B.F., and Hackett, W.R., 1984, Strombolian and phreatomagmatic deposits of Ohakune Craters, Ruapehu, New Zealand—a complex interaction between external water and rising basaltic magma: *Journal of Volcanology and Geothermal Research*, v. 21, p. 207–231.
- Houghton, B.F., and Nairn, I.A., 1991, The 1976–1982 strombolian and phreatomagmatic eruptions of White Island, New Zealand—eruptive and depositional mechanisms at a 'wet' volcano: *Bulletin of Volcanology*, v. 54, p. 25–49.
- Houghton, B.F., and Schmincke, H.-U., 1989, Rothenberg scoria cone, East Eifel—a complex Strombolian and phreatomagmatic volcano: *Bulletin of Volcanology*, v. 52, p. 28–48.
- Houghton, B.F., and Smith, R.T., 1993, Recycling of magmatic clasts during explosive eruptions—estimating the true juvenile content of phreatomagmatic volcanic deposits: *Bulletin of Volcanology*, v. 55, p. 414–420.
- Houghton, B.F., and Wilson, C.J.N., 1989, A vesicularity index for pyroclastic deposits: *Bulletin of Volcanology*, v. 51, p. 451–462.
- Ishihara K., 1985, Dynamical analysis of volcanic explosion: *Journal of Geodynamics*, v. 3, p. 327–349.
- Jorgensen, T.P., 1993, *The physics of golf*: New York, American Institute of Physics, and Oxford University Press, 155 p.
- Lorenz, V., 1970, Some aspects of the eruption mechanism of the Big Hole Maar, central Oregon: *Geological Society of America Bulletin*, v. 81, p. 1823–1830.
- Lorenz, V., 1974, Studies of the Surtsey tephra deposits: *Surtsey Research Progress Report*, v. 7, p. 72–79.
- Lorenz, V., and Büchel, G., 1980, Zur Vulkanologie der Maare und Schlackenkegel der Westeifel: *Mitt. Pollichia*, v. 68, p. 29–100.
- Lorenz, V., and Zimanowski, B., 1984, Fragmentation of alkali-basalt magmas and wall-rocks by explosive volcanism: *Annals of Science, University of Clermont-Ferrand [France]*, v. 74, p. 15–25.
- Mastin, L.G., 1991, The roles of magma and groundwater in the phreatic eruptions at Inyo Craters, Long Valley caldera, California: *Bulletin of Volcanology*, v. 53, p. 579–596.
- Mastin, L.G., 1995, Thermodynamics of gas and steam-blast eruptions: *Bulletin of Volcanology*, v. 57, p. 85–98.
- Minakami, T., 1942, On the distribution of volcanic ejecta, Part I, the distributions of volcanic bombs ejected by the recent explosions of Asama: *Bulletin of the Earthquake Research Institute, Tokyo*, v. 20, p. 65–91.
- Mironer, A., 1979, *Engineering fluid mechanics*: New York, McGraw-Hill, 592 p.

- Nairn, I.A., 1976, Atmospheric shock waves and condensation clouds from Ngauruhoe explosive eruptions: *Nature*, v. 259, p. 190–192.
- Nairn, I.A., and Self, S., 1978, Explosive eruptions and pyroclastic avalanches from Ngauruhoe in February 1975: *Journal of Volcanology and Geothermal Research*, v. 3, p. 39–60.
- Peckover, R.S., Buchanan, D.J., and Ashby, D.E.T.F., 1973, Fuel-coolant interactions in submarine vulcanism: *Nature*, v. 245, p. 307–308.
- Rosi, M., and Santacroce, R., 1983, The A.D. 472 "Pollena" eruption—volcanological and petrological data for this poorly-known plinian-type event at Vesuvius: *Journal of Volcanology and Geothermal Research*, v. 17, p. 249–271.
- Rosi, M., Principe, C., and Vecci, R., 1993, The 1631 Vesuvius eruption—a reconstruction based on historical and stratigraphical data: *Journal of Volcanology and Geothermal Research*, v. 58 p. 151–201.
- Rouse, H., 1946, *Elementary mechanics of fluids*: New York, John Wiley (republished 1978 by Dover Publications, New York), 376 p.
- Self, S., Kienle, J., and Huot, J.-P., 1980, Ukinrek Marrs, Alaska, 11—deposits and formation of the 1977 craters: *Journal of Volcanology and Geothermal Research*, v. 7, p. 39–65.
- Sheridan, M.F., Barberi, F., Rosi, M., and Santacroce, R., 1981, A model for plinian eruptions of Vesuvius: *Nature*, v. 289, p. 282–285.
- Sigurdsson, H., Carey, S., Cornell, W., and Pescatore, T., 1985, The eruption of Vesuvius in A.D. 79: *National Geographic Research*, v. 1, p. 332–387.
- Sparks, R.J.S., 1986, The dimensions and dynamics of volcanic eruption columns: *Bulletin of Volcanology*, v. 48, p. 3–15.
- Steinberg, G.S., and Lorenz, V., 1983, External ballistic of volcanic explosions: *Bulletin of Volcanology*, v. 46, p. 333–348.
- Voight, B., 1981, Time scale for the first moments of the May 18 eruption, in Lipman, P.W. and Mullineaux, D.R., *The 1980 eruptions of Mount St. Helens*, Washington: U.S. Geological Survey Professional Paper 1250, p. 69–86.
- Waite, R.B., Hansen, V.L., Sarna-Wojcicki, A.M., and Wood, S.H., 1981, Proximal air-fall deposits of eruptions between May 24 and August 7, 1980—stratigraphy and field sedimentology, in Lipman, P.W., and Mullineaux, eds., *The 1980 eruptions of Mount St. Helens*, Washington: U.S. Geological Survey Professional Paper 1250, p. 617–628.
- Walker, G.P.L., Wilson, L., and Howell, E.L.G., 1971, Explosive volcanic eruptions—I, The rate of fall of pyroclasts: *Geophysical Journal of the Royal Astronomical Society*, v. 22, p. 377–383.
- Wagh, J.G., and Stubbard, G.W., 1973, Hydroballistic modeling: San Diego, U.S. Naval Undersea Center (now Naval Command, Control, and Ocean Surveillance Center), 348 p.
- White, E.M., 1979, *Fluid mechanics*: New York, McGraw Hill, 701 p.
- Williams, H., and McBirney, A.R., 1979, *Volcanology*: San Francisco, Freeman, Cooper & Co., 397 p.
- Wilson, L., 1972, Explosive volcanic eruptions—11, the atmospheric trajectories of pyroclasts: *Geophysical Journal of the Royal Astronomical Society (London)*, v. 30, p. 381–392.
- Wilson, L., 1980, Relationships between pressure, volatile content, and ejecta velocity in three types of volcanic explosion: *Journal of Volcanology and Geothermal Research*, v. 8, p. 297–313.
- Wohletz, K.H., 1983, Mechanisms of hydrovolcanic pyroclast formation—grain-size, scanning electron microscopy, and experimental studies: *Journal of Volcanology and Geothermal Research*, v. 17, p. 31–63.
- Wohletz, K.H., and McQueen, R.G., 1984, Volcanic and stratospheric dustlike particles produced by experimental water-melt interactions: *Geology*, v. 12, p. 591–594.
- Woods, A.W., 1988, The fluid dynamics and thermodynamics of eruption columns: *Bulletin of Volcanology*, v. 50, p. 169–193.